that of the lamp (in the region transmitted by the monochromator).

The average cesium density calculated from these pictures shows a discrepancy with the density calculated from the amount of cesium injected (see Table 1). In the latter case a uniform distribution is assumed, which is certainly not the case. For this calculation the width of the channel is taken from wall to wall. However, in the former case the line of sight between the two sapphire windows is much larger. Both effects lead to a higher value of the cesium density for the absorption measurement. This is confirmed by the results given in Table 1. The increasing discrepancy between columns 1 and 3 for the last three runs is explained by the decreasing window transparency, which leads to larger experimental uncertainties. During the last 15 runs of the measurement series this transparency decreased by a factor of more than 100 for a pair of windows.

Pictures made from the signals recorded directly on the Ampex show an unexpected behavior (see Figs. 4 and 5). There are large fluctuations in the absorption signal on a time scale of 1 ms. These fluctuations are present with and without power extraction. Fourier transforms of the signals show a more or less constant spectrum between 30 and 1000 Hz and a rapid decay beyond 1 kHz. Figures 4 and 5 show two signals: a) before cesium addition and b) during power extraction. From $t = 0$ to $t = 16$ ms the chopper is open; beyond $t = 16$ ms the chopper is closed, and no light from the generator is recorded. In Fig. 4 the signal is filtered at 30 kHz, in Fig. 5 at 1 kHz. The high-frequency noise in Fig. 4 originates from the tape recorder. The cesium density corresponding to the maximum and minimum of the absorbed signal varies by a factor of two.

V. Conclusion

Replacing a high-pressure xenon lamp as a light source for absorption measurements by a GaAlAs laser diode yields a substantial improvement. Temperature stabilization with the built-in Peltier element and thermistor is easily achieved. The single mode with the highest intensity is selected with a monochromator. The stability of the output power in this single mode is better than 1% for several hours. The spectral output power density is about 100 times higher than that of the xenon lamp. The spontaneous emission of the plasma is not detected when the diode laser is used as the source in a cesium density measurement in an MHD generator. This allows a determination of the cesium density during the power extraction, and the signal is strong enough to obtain a high time resolution. A demonstration of the power of this measurement is the observation of fluctuations of a factor of two in the cesium density, within a millisecond, in an MHD generator during power extraction.

Acknowledgments

This work was performed with financial support from the Netherlands Department of Economic Affairs and the Stichting voor de Technische Wetenschappen (STW). The author wishes to thank R. Damstra, A. P. C. Holten, and C. H. F. M. van de Weem for their valuable contributions to the experiments; also, the author wishes to acknowledge the helpful discussions with W. F. H. Merck, L. H. Th. Rietjens, and A. Veefkind.

References

[1]van Veldhuizen, E. M., and Flinsenberg, H. J., "Methods and Results of Diagnosis in a Closed-Cycle MHD Blowdown Generator," *Journal of Propulsion and Power,* Vol. 3, No. 6, Nov. 1987, pp. 542–551.

[2]Chen, C. L., and Phelps, A. V., "Absorption Coefficients for the Wings of the First Two Resonance Doublets of Cesium Broadened by Argon," *Physical Review,* Vol. A7(2), Feb. 1972, pp. 470–479.

[3]van Veldhuizen, E. M., and Holten, A.P.C., "An Overview of Diagnostic Results of the EUT Blow-Down Generator," *Proceedings of the 26th Symposium on Engineering Aspects of Magnetohydrodynamics,* Nashville, TN, 1988, pp. 9.3.1–9.3.8.

[4]Balemans, W.J.M., and Rietjens, L.H.T., "High Enthalpy Extraction Experiments with the Eindhoven Blow-Down Facility," *Proceedings of the 9th International Conference on MHD Electrical Power Generation,* Vol. 2, Tsukuba, Japan, 1986, pp. 230–240.

[5]Balemans, W.J.M., Massee, P., and Rietjens, L.H.T., "Construction and Operation of the Eindhoven MHD Blow-Down Facility," *Proceedings of the 26th Symposium on Engineering Aspects of Magnetohydrodynamics,* Nashville, TN, 1988, pp. 2.4.1–2.4.8.

Steady Flow Combustion Model for Solid-Fuel Ramjet Projectiles

Michael J. Nusca*
U.S. Army Ballistic Research Laboratory, Aberdeen Proving Ground, Maryland

Nomenclature

c_p	= specific heat at constant pressure
h	= heat of formation
h_{vap}	= heat of vaporization per unit mass
$\tilde{h}$	= total enthalpy
k	= turbulence kinetic energy
M	= molecular weight
m	= mass fraction
$\dot{m}$	= mass flow rate
n	= stoichiometric air/fuel mass ratio
$\hat{n}$	= normal direction
p	= static pressure
q	= heat flux
$\Re$	= universal gas constant
R	= reaction rate per unit volume
r	= radial direction
$\dot{r}$	= solid fuel regression rate
Sc	= Schmidt number
T	= temperature
u	= velocity component in the axial direction
V	= magnitude of the local velocity vector
v	= velocity component in the azimuthal direction
w	= velocity component in the radial direction
z	= axial direction
Γ	= diffusion coefficient, μ_{eff}/Sc
ϵ	= turbulence dissipation rate
κ	= thermal conductivity
μ	= viscosity
ρ	= density
ϕ	= general flow variable
ψ	= stream function
ω	= vorticity

Subscripts

eff	= effective
fo	= fuel-oxidizer
fp	= fuel-products
fu	= fuel

Presented as Paper 89-2797 at the AIAA 25th Joint Propulsion Conference, Monterey, CA, July 10–12, 1989; received April 20, 1989; revision received Aug. 2, 1989.

*Aerospace Engineer, Launch and Flight Divisoin. Member AIAA.

inlet	= at the inlet
j	= jth mixture component
k	= turbulence kinetic energy
op	= oxidizer-products
ox	= oxidizer
pr	= products
t	= turbulent
vap	= vaporization
wall	= on the wall

Introduction

VARIOUS solid-fuel ramjet (SFRJ) tubular projectiles have been developed by the U.S. Army Ballistic Research Laboratory (BRL).[1] One of these projectiles, a spin-stabilized 75-mm version (see Fig. 1), has been designed and tested for use as a tank gun training round (TGTR) for the 105-mm, M68 tank cannon. The concept of the TGTR is to use the thrust (hence low drag) of the SFRJ projectile to obtain a ballistic match with low drag kinetic energy projectiles up to 3 km in range. Upon depletion of the propellant and choking of the internal flow, the SFRJ will become a high-drag projectile with limited range.

Several wind tunnel tests were conducted by the BRL Launch and Flight Division using unfueled, nonspinning, full-scale SFRJ models.[2] These tests provided internal surface pressure measurements for a variety of configurations at a freestream Mach number of 4.03. Subsequently, Nusca et al.[3] used a zonal computational fluid dynamics (CFD) code to compute the nonreacting, internal flowfield for several 75-mm SFRJ internal configurations. These computed results compared favorably with measured internal wall pressure data. Recently, this code has been extended to finite-rate chemistry.[4] As an initial step to examine solid fuel combustion in the SFRJ, a subsonic flow code and mass-controlled combustion model were developed.[5] This combustion model does not require reaction rates, which are not well determined for solid fuels used in the SFRJ projectile. Using a very fine grid, the present code requires about 0.5 CPU h/solution on a CRAY X-MP/48 computer. The code is therefore suitable for SFRJ combustor design studies.

The governing equations (derived in Ref. 5) for stream function, vorticity, azimuthal velocity, stagnation enthalpy, and species mass fraction can be expressed in the form of a general variable ϕ. For the present study, the local flow velocity was constrained to be smaller than the local speed of sound. Thus the governing equations are elliptic. Since the SFRJ geometry is axisymmetric, the equations are cast in an r,z coordinate system and in axisymmetric form.

$$a_\phi\left[\frac{\partial}{\partial z}\left(\phi\frac{\partial\psi}{\partial r}\right)-\frac{\partial}{\partial r}\left(\phi\frac{\partial\psi}{\partial z}\right)\right]-\frac{\partial}{\partial z}\left[b_\phi r\frac{\partial}{\partial z}(c_\phi\phi)\right]$$

$$-\frac{\partial}{\partial r}\left[b_\phi r\frac{\partial}{\partial r}(c_\phi\phi)\right]+rd_\phi=0 \tag{1}$$

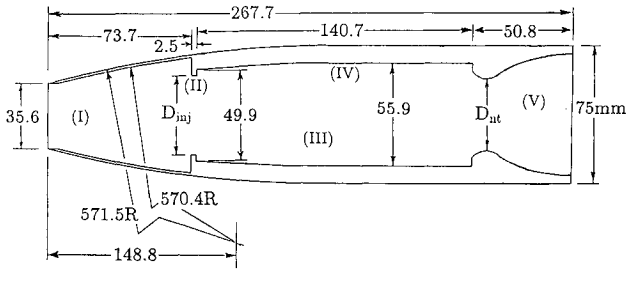

Fig. 1 SFRJ Geometry; D_{inj} = 43.2 mm, D_{nt} = 40.6 mm; (I) inlet, (II) injector, (III) combustion chamber, (IV) fueled wall, (V) nozzle.

The parameters a_ϕ, b_ϕ, c_ϕ, and d_ϕ are given in Ref. 5. The equations of state are

$$\tilde{h}=T\sum_j c_{p_j}m_j+\sum_j h_j m_j+\frac{V^2}{2}+k \tag{2}$$

$$\rho=\frac{p/\Re T}{\Sigma_j(m_j/M_j)}=\frac{p/\Re}{\tilde{h}-(V^2/2)-k-\Sigma_j h_j m_j}\cdot\frac{\Sigma_j c_{p_j}m_j}{\Sigma_j(m_j/M_j)} \tag{3}$$

The solution scheme, based on central differencing for the diffusive and source terms, upwind differencing for the convective terms, and a Gauss-Seidel relaxation algorithm, is described in Ref. 5. Convergence is satisfied when the greatest relative change in any flow variable, ϕ, over the all grid points, is smaller than a prescribed tolerance.

In these equations the shear stress includes the Reynolds stress with an effective fluid viscosity (μ_{eff}) expressed as the sum of the molecular and turbulent viscosities. The turbulent fluid properties are being treated as kinematic properties with a set of augmented transport coefficients denoted "eff." The calorically perfect gas assumption is made since the temperature dependence of c_{p_j} for the reactants and products is not well determined for some solid fuels. The Prandtl and Schmidt numbers are assumed to be unity. Static pressure at any point in the flowfield is computed by integrating the radial and axial momentum equations from the prescribed chamber inlet (or exit) value. See Ref. 5 for further details.

Combustion Model

Many of the assumptions commonly made in combustion models are also incorporated into the present model. In particular, assumptions made in the Shvab-Zeldovich formulation.[6] The reacting fluid is treated as a continuum with equal mass diffusivity properties for all species. The specific heat at constant pressure of each species is assumed constant in the gas phase. The reacting solid surface is considered energetically homogeneous (i.e., gas-solid interface effects are neglected). Radiation energy transfer is neglected. A one-step, irreversible, mass-controlled (i.e. fixed stoichiometric ratio, n) reaction is considered for which the reactants are fully consumed. The products are considered a single specie.

$$\text{fuel}+n\ \text{oxidizer}\rightarrow(1+n)\ \text{products}$$

The reaction flame is considered to be nonpremixed, steady, nearly isobaric, and of zero thickness, i.e., a diffusion flame.[6] The reaction rate is considered to be much faster than the rate of diffusion so that the reaction is diffusion controlled. Studies on this and similar models for combustion chamber flows have been performed.[6-8] In addition, the steady nature of solid fuel ramjet combustion has been demonstrated experimentally.[7]

The mass conservation of fuel and oxidizer [see Eq. (1)] are expressed as

$$\frac{\partial}{\partial z}\left[m_{\text{fu}}\frac{\partial\psi}{\partial r}\right]-\frac{\partial}{\partial r}\left[m_{\text{fu}}\frac{\partial\psi}{\partial z}\right]-\frac{\partial}{\partial z}\left[(\Gamma_{\text{fu}})_{\text{eff}}\,r\frac{\partial m_{\text{fu}}}{\partial z}\right]$$

$$-\frac{\partial}{\partial r}\left[(\Gamma_{\text{fu}})_{\text{eff}}\,r\frac{\partial m_{\text{fu}}}{\partial r}\right]-rR_{\text{fu}}=0 \tag{4}$$

$$\frac{\partial}{\partial z}\left[m_{\text{ox}}\frac{\partial\psi}{\partial r}\right]-\frac{\partial}{\partial r}\left[m_{\text{ox}}\frac{\partial\psi}{\partial z}\right]-\frac{\partial}{\partial z}\left[(\Gamma_{\text{ox}})_{\text{eff}}\,r\frac{\partial m_{\text{ox}}}{\partial z}\right]$$

$$-\frac{\partial}{\partial r}\left[(\Gamma_{\text{ox}})_{\text{eff}}\,r\frac{\partial m_{\text{ox}}}{\partial r}\right]-rR_{\text{ox}}=0 \tag{5}$$

For a general multistep reaction, R_{fu} and R_{ox} are difficult to accurately determine. Indeed, the uncertainty in these data places a severe restriction on the accuracy of the entire computation. However, for the one-step reaction described above,

the reaction rates are related

$$R_{fu} = R_{ox}/n \quad R_{fu} = -R_{pr}/(1+n) \quad R_{ox}/n = -R_{pr}/(1+n)$$

The R terms can be eliminated from Eqs. (4) and (5) by dividing Eq. (5) by n and subtracting the resultant equation from Eq. (4). In addition, fuel and oxidizer are assumed to have identical diffusion properties so that $\Gamma_{fu} = \Gamma_{ox} \equiv \Gamma_{fo}$.

$$\frac{\partial}{\partial z}\left[\phi_{fo}\frac{\partial \psi}{\partial r}\right] - \frac{\partial}{\partial r}\left[\phi_{fo}\frac{\partial \psi}{\partial z}\right] - \frac{\partial}{\partial z}\left[r(\Gamma_{fo})_{eff}\frac{\partial \phi_{fo}}{\partial z}\right] - \frac{\partial}{\partial r}\left[r(\Gamma_{fo})_{eff}\frac{\partial \phi_{fo}}{\partial r}\right] = 0 \tag{6}$$

where $\phi_{fo} \equiv m_{fu} - m_{ox}/n$. Assuming that $\Gamma_{fu} = \Gamma_{pr} \equiv \Gamma_{fp}$ and $\Gamma_{ox} = \Gamma_{pr} \equiv \Gamma_{op}$, then Eq. (6) can be written in terms of $\phi_{fp} \equiv m_{fu} + m_{pr}/(1+r)$ or $\phi_{op} \equiv m_{ox}/n + m_{pr}/(1+n)$, as well.

Turbulence Model

Modeling the effective viscosity $\mu_{eff} = \mu + \mu_t$ for a turbulent, reacting flow has been the subject of much investigation.[5,6] Use of a two-equation model, e.g., $k-\epsilon$, for reacting flow relies on an adequate formulation of the source terms in these equations. In contrast, a closed-form phenomenological model for the effective viscosity in a confined, turbulent, steady diffusion flame can be used. One such model was proposed by Pun and Spalding.[9]

$$\mu_{eff} = KD^{2/3}L^{-1/3}\rho^{2/3}[\dot{m}u^2 + \dot{m}(rv)^2]^{1/3}_{inlet} \tag{7}$$

where K is a constant and is chosen to insure a prescribed value of μ_{eff} at the inlet. The parameters D and L are the maximum diameter and length of the combustion chamber, respectively. The inlet swirl velocity is rv. This model assumes that μ_{eff} increases with ρ, D, and the momentum (or kinetic energy) of the fluid entering the chamber (including flow swirl), but decreases with increasing chamber length, L. Use of an algebraic model without the solution of an equation for the turbulence kinetic energy k necessarily neglects the contribution of k to the total enthalpy [see Eq. (2)].

Boundary Conditions

At the inlet plane, radial profiles of all dependent variables ($\psi, \omega, v, \tilde{h}$, and m_j) as well as values for T, p, ρ, and μ_{eff} are specified. It is assumed that the flow at the inlet plane consists of air ($m_{ox} = 1$, $m_{fu} = 0$) and that the combustion process does not effect the inlet flow. The exit plane is located at the nozzle throat where the flow is assumed to be subsonic. Since the nozzle is extended by a short constant-diameter aft section, the streamlines at the exit plane are parallel to the symmetry axis; thus flow gradients along the streamlines are zero. The symmetry axis is considered to be a streamline of the flow. The no-slip condition is applied to all walls (i.e., $u = w = 0$, $v = \Omega r$, where Ω is the chamber rotation rate). For an inert (unfueled) wall the normal gradient of all mass fractions $\partial m_j/\partial \hat{n}$ are set to zero and the wall is adiabatic. The fueled wall is considered to be a source of fuel ($m_{fu} = 1$, $m_{ox} = 0$), with a wall temperature equal to the vaporization temperature of the fuel $T_{wall} = T_{vap}$. In this case the fuel is in a vapor state and is diffused instead of injected from the wall (at a prescribed injection velocity). The regression rate on the fueled wall is determined from the temperature gradient normal to the wall,[7]

$$\dot{r} = \frac{q_{wall}}{\rho_{wall}\bar{h}_{vap}} \tag{8}$$

where q_{wall} is the local heat flux to the wall ($-\kappa \partial T/\partial \hat{n})_{wall}$, and ρ_{wall} is the density of the fuel. Values of the thermal conductivity, density, and heat of vaporization are available for most solid fuels.

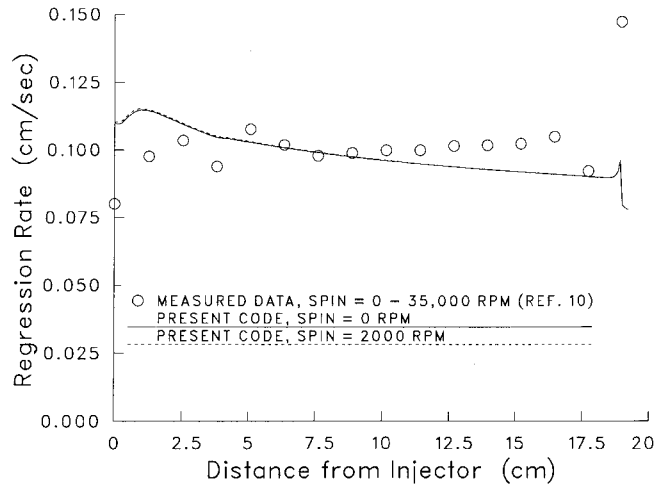

Fig. 2 Regression rate distribution along the fueled wall of an SFRJ; connected-pipe test, HTPB fuel.

Results and Discussion

The computational fluid dynamics code and combustion model were used to simulate the reacting flow in the axisymmetric combustion chamber of a 75-mm SFRJ projectile (see Fig. 1). The computational grid and grid refinement investigations are described in Ref. 5. The wall spacing used for these computations was approximately 0.012 chamber diameters. Converged solutions were obtained after about 800 iterations and approximately 15 min of CPU time on a CRAY X-MP/48 computer. No under-relaxation was required.

Computations are presented for 43.2-mm (1.7-in.) injector and 40.6-mm (1.6-in.) nozzle throat diameters. Nonreacting flow computations[3] for a 27.9-mm (1.1-in.) nozzle diameter show that the flow velocity, pressure, density, and temperature are nearly constant across the entrance to the combustion chamber (except very close to the wall). The smaller nozzle diameter is used to produce subsonic combustor entrance flow. Average values for these flow variables are considered sufficient upstream conditions for the present simulation.[5] The Reynolds number is 9.8×10^6/m based on the entrance flow.

The solid fuel consists of four main components: 30% ammonium perchloride (AP), 28.5% hydroxl-terminated polybutadiene (HTPB), 40% Escorez, and 1.5% Catocene. The molecular weight of the fuel is 97.7 g/mole. The oxidizer is air with a molecular weight of 28.8 g/mole. The main products of combustion are hydrocarbon, oxygen, water and nitrogen, assuming 67% CH_2, 16.3% O_2, 12.1% H_2O, and 4.9% N_2. The combined molecular weight of the product is 18.2 g/mole. The fuel density, heat of vaporization, vaporization temperature, and stoichiometric air/fuel ratio are 1.189 g/cm^3 (74.2 lb/ft^3), 2.8998×10^7J/kg (12465.6 Btu/lb), 1755°R, and 9.152, respectively.

Holzman et al.[10] have measured the solid fuel regression rate in a 75-mm SFRJ projectile using a connected-pipe test stand. A typical inlet mass flux for the test was 1814 g/s (4 lb/s) at an inlet velocity of approximately 98 m/s (323 ft/s) and a temperature of 1850°R. Measurements were made for combustor axial spinrates up to 35,000 rpm (3665 rad/s). The solid fuel regression rate was determined from the measured fuel grain regression and the test run time. Figure 2 shows the fuel regression rate distribution along the fueled wall. In this case, the solid fuel did not contain AP, and the effect of chamber axial spin was found to be insignificant. The present computations for solid fuel without AP reproduce overall fuel regression rates reasonably well. At the beginning of the fuel grain behind the injector, the computed regression rate is larger than measured. However, the overall trends, including the peak regression rate at the flow reattachment point, are similar. There are two possible explanations for this dis-

crepancy. In the recirculating flow, radiation effects are very significant[6] but are ignored in the present code. Turbulence modeling for the recirculating flow in SFRJ combustors is difficult,[3] even without combustion-generated turbulence, and may not be properly modeled using the present code. At the end of the combustor, only the trend of increased regression rate is simulated. In this region the fuel grain joins the nozzle producing a corner flow. Possible errors in the specified wall boundary conditions, errors in turbulence modeling, or the neglecting of soot production for HTPB fuel may explain the discrepancy.

Figure 3 shows typical computed temperature and product mass fraction profiles across the SFRJ combustor at about the midpoint between the inlet and nozzle. The maximum temperature of about 4300°R and the maximum product mass fraction of 1 are found at the flame location, about 70% chamber radius. On the fueled wall, the temperature is held at 1755°R, and the mass fraction of product is zero. Temperature and mass fraction gradients on both sides of the flame are large. The chamber centerline temperature is equivalent to the inlet air value, and the mass fraction of product is zero.

Elands et al.[7] have also measured the solid fuel regression rate in an SFRJ chamber using a connected-pipe test facility. Polyethylene (PE) fuel was used in a small-scale SFRJ configuration. The inlet diameter was 15 mm (0.6 in.), and the maximum chamber diameter was 45 mm (1.8 in.). Measurements of local regression rate on the fuel gain were taken using a nonintrusive ultrasonic method. For comparison to the present code, the values of fuel molecular weight, density, vaporization temperature, and heat of vaporization were taken as 28.05 g/mole (C_2H_4), 0.8008 g/cm^3 (50.0 lb/ft^3), 1440°R, and 4.0009×10^6 J/kg (1719.9 Btu/lb), respectively. The inlet air temperature was 540°R. Figure 4 shows that the average fuel regression rate, over the fuel gain length, increases as the inlet air mass flow rate is increased. The results of a finite-rate chemistry code, reported in Ref. 7, and the present diffusion-flame code are also shown. The present code does not require thermodynamic burning rates for the PE fuel. Reaction rates for PE are available for finite-rate models. Both combustion models reproduce the trend and magnitude of the data. The computational grid used by the present code, 338×44, was more dense than the grid used by the finite-rate code, 20×20.

Mermagen and Yalamanchili[1] have conducted free-flight tests of fin-stabilized (FS) 75-mm SFRJ projectiles with HTPB solid fuel. A Hawk radar/Doppler velocimeter was used to measure the velocity and drag vs range for projectiles with different injector and nozzle throat diameters and solid fuels

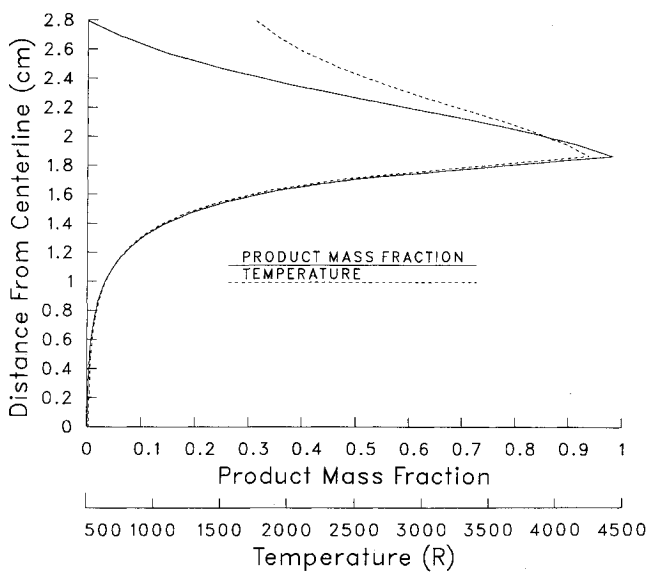

Fig. 3 Computed product mass fraction and temperature profiles for a SFRJ at approximate midlength; HTPB fuel.

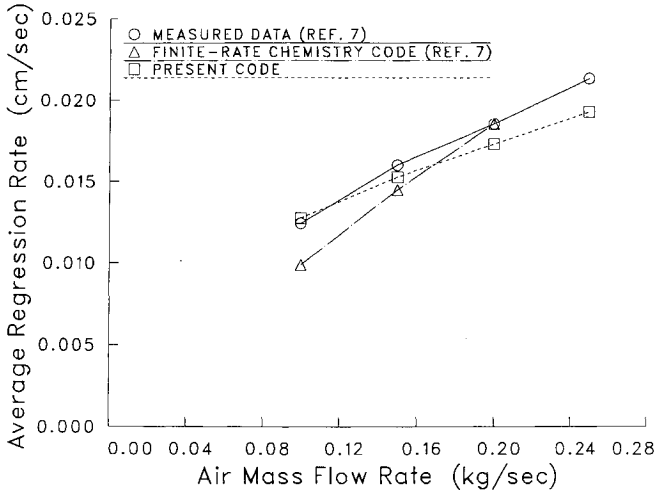

Fig. 4 Variation of fuel regression rate with air mass flow rate in an SFRJ combustor; polyethylene fuel.

(including inert projectiles). The SFRJ thrust is defined from this data using the difference in drag coefficient, ΔC_D, between fueled and unfueled SFRJ projectiles at the same Mach number. The FS-SFRJ projectile generates about 1112 N (250 lb_f) of thrust during the 1.6 s burn time. The solid fuel in these projectiles contains AP. The FS-SFRJ has a longer combustion chamber (fuel gain) than the spin-stabilized version. In addition, the FS-SFRJ has nearly zero axial spin in flight.

The present steady-state combustion model can predict the FS-SFRJ burn time from the solid fuel regression rate ($\dot{r}$) and the thickness of the solid fuel layer. The drag coefficient for the combustion chamber is computed using the change in momentum from the chamber inlet to the nozzle exit. Computations reported in Ref. 3 were used for the exterior and inlet (unfueled section) drag. Although the projectile decelerates during the burn, the computation assumes a steady-state burn and thus the launch velocity of 1372 m/s (Mach 4.03) is used. The computed burn time is 1.9 s, 18% longer than the 1.6 s observed. The computed thrust is 934 N (210 lb_f), 16% smaller than the average measured thrust of 1112 N. Since fuel oxidizer (AP) effects are not included in the combustion model the computation overestimates the burn time and underestimates the thrust. Flight tests of solid fuels without AP in SFRJ projectiles have not been reported. However, connected-pipe tests[10] show that the addition of AP (with catalyst) to HTPB solid fuel increases the regression rate (and decreases the burn time) by about 40% in a nonspinning SFRJ. Thrust measurements are not available, however, AP should increase the thrust generated by an SFRJ due to an increased fuel flow rate. Sources of discrepancy between measured and computed flight performance include the effects of radiation and soot production which are excluded from the combustion model, uncertainty in the thermodynamic input quantities, and the validity of the diffusion-flame model. Efforts should be made to incorporate the effects of AP for nonspinning flight cases.

Conclusions

A steady-flow solution of the Navier-Stokes equations is linked with a diffusion-flame combustion model for a one-step, irreversibly, mass-controlled reaction between solid fuel and air. The reactants are completely consumed, and the products are treated as a single specie. A one-equation, algebraic turbulence model for combustor flows is employed. Solutions produced by this code are applied to the subsonic flow, solid-fuel combustion within a SFRJ projectile. The results provide estimates of the major features of the internal flow including solid fuel regression rate, burn time, and thrust. Burn time and thrust predictions compare favorably with flight test data. Since the code assumes a mass-controlled

reaction, reaction rate data is not required. Thus the code can be applied to the wide range of solid fuels commonly used in SFRJ design. The application of a simplified combustion model serves as a logical first step in modeling the reacting flow in SFRJ projectiles, without introduction of the uncertainties in reaction rates and detailed turbulence modeling. The addition of radiation, soot production, and fuel oxidizer (AP) effects could improve the utility of the simulation.

References

[1]Mermagen, W. H., and Yalamanchili, R. J., "Experimental Tests of a 105/75 mm Solid Fuel Ramjet Tubular Projectile," U.S. Army Ballistic Research Laboratory, Aberdeen Proving Ground, MD, ARBRL-MR-3416, Dec. 1984.

[2]Kayser, L. D., Yalamanchili, R. J., and Trexler, C., "Pressure Measurements on the Interior Surface of a 75 mm Tubular Projectile at Mach 4," U.S. Army Ballistic Research Laboratory, Aberdeen Proving Ground, MD, ARBRL-MR-3725, Dec. 1988.

[3]Nusca, M. J., Chakravarthy, S. R., and Goldberg, U. C., "Computational Capability for the Solid Fuel Ramjet Projectile," U.S. Amry Ballistic Research Laboratory, Aberdeen Proving Ground, MD, ARBRL-TR-2958, Dec. 1988; (also, Goldberg, U. C., Chakravarthy, S. R., and Nusca, M. J., "A New Computational Capability for Ramjet Projectiles," AIAA Paper 87-2411, Aug. 1987).

[4]Palaniswamy, S., and Chakravarthy, S. R., "Finite Rate Chemistry for USA-Series Codes: Formulation and Applications," AIAA Paper 89-0200, Jan. 1989.

[5]Nusca, M. J., "Steady Flow Combustion Model for Solid-Fuel Ramjet Projectiles," U.S. Army Ballistic Research Laboratory, Aberdeen Proving Ground, MD, ARBRL-TR-2987, April 1989; also, AIAA Paper 89-2797, July 1989.

[6]Williams, F. A., *Combustion Theory*, Addison-Wesley, Reading, MA, 1965.

[7]Elands, P. J. M., Korting, P. A. O. G., Dijkstra, F., and Wijchers, T., "Combustion of Polyethylene in a Solid Fuel Ramjet—A Comparison of Computational and Experimental Results," AIAA Paper 88-3043, Jan. 1988.

[8]Netzer, D. W., "Modeling Solid-Fuel Ramjet Combustion," *Journal of Spacecraft and Rockets*, Vol. 14, No. 12, Dec. 1977, pp. 762–766.

[9]Pun, W. M., and Spalding, D. B., "A Procedure for Predicting the Velocity and Temperature Distributions in a Confined, Steady, Turbulent, Gaseous, Diffusion Flame," Mechanical Engineering Dept., Imperial College, London, Rept. SF/TN/11, 1967.

[10]MacLaren, R. O., and Holzmann, A. L., "SFRJ Projectile Development," United Technologies Corp., Chemical Systems Div., Sunnyvale, CA, CSD-2710-FR, June 26, 1981; also, Holzmann, A. L., and Husain, S. M., "Spin Phenomenology," United Technologies Corp., Chemical Systems Div., Sunnyvale, CA, IR&D Rept., Nov. 1988.